Journal of Engineering Mathematics **50:** 359–378, 2004.

The propagation and basal solidification of two-dimensional and axisymmetric viscous gravity currents

WARREN R. SMITH
School of Mathematics and Statistics, The University of Birmingham, Edgbaston, Birmingham, B15 2TT, U.K.

Received 12 March 2003; accepted in revised form 7 July 2004

Abstract. The effect of basal solidification on viscous gravity currents is analysed using continuum models. A Stefan condition for basal solidification is incorporated into the Navier-Stokes equations. A simplified version of this model is determined in the lubrication and large-Bond-number limit. Asymptotic solutions are obtained in three parameter régimes. (i) A similarity solution is possible in the following cases: the two-dimensional problem when volume per unit length (V) is proportional to time (t) raised to the power $7/4 (V = qt^{7/4})$ and the Julian number ($\nu^3 g^2/q^4$) is large, where ν is kinematic viscosity, q is a constant of proportionality and g is the acceleration due to gravity; the axisymmetric problem when volume is proportional to time raised to the power 3 ($V = Qt^3$) and the dimensionless group $\nu g/Q$ is large, where Q is a constant of proportionality. In both cases, the front is found to depend on time raised to the power 5/4, as it does in the absence of solidification, but the constant of proportionality satisfies a modified system of equations. (ii) In the case of large Stefan number and small modified Peclet number ($\mathrm{Pe}\delta^2 \ll 1$, where Pe is the Peclet number and δ is the aspect ratio), asymptotic and numerical methods are combined to produce the most revealing results. The temperature of the fluid approaches the melting point over a short time-scale. Over the long time-scale, the solid/liquid interface is determined from the conduction of latent heat into the solid. Strong coupling is observed with the basal solidification modifying the flow at leading order. The solidification may retard and eventually arrest the front motion long before complete phase change has taken place. (iii) In the case of constant volume and large modified Peclet number ($\mathrm{Pe}\delta^2 \gg 1$), similarity solutions are found for the solidification at the base of the gravity current on the short time-scale. The coupling is weak on this time-scale with the solidification being dependent on the front position but not influencing the fluid motion at leading order. Over the long time-scale, the drop completely solidifies. Analytical solutions are not obtained on this time-scale, but scalings are deduced.

Key words: basal solidification, coupled moving boundary problem, viscous gravity current

1. Introduction

The effect of basal solidification on the dynamics of the gravity current has not been extensively investigated. We begin by reviewing some related studies. The spreading of viscous gravity currents without solidification has received a great deal of attention over several decades (see, for example, [1–3]). This is due to its relevance for geophysical flows and for nuclear safety considerations. A limited number of articles have appeared which concern spreading and basal solidification. An experimental study at low Bond number when the spreading is driven by capillary action was described in [4]. The retarding and the arrest of the front was observed in experiments performed at small Bond number. In an appendix of [3], a model for spreading and basal solidification was stated. The thermal conduction time-scale was assumed to be much smaller than the spreading and solidification time-scales; this simplifying assumption is not required in this article. A similar study to the work described in this article at large Bond number was presented by Bunk [5]. However, the latent heat and heat conduction in the solid were not considered and we address these issues here. Bunk concludes that latent

heat is of minor importance for large-Prandtl-number melts. We show that this conclusion is only true on the short time-scale. The basal solidification of an inertia-dominated flow, which recently arose in the study of laser percussion drilling (see [6]), has features in common with the current application. Several of the developments made in this laser-drilling application are incorporated here.

In this paper, the flow of a liquid melt between a gas and a solid base is considered. Our attention is restricted to the problem where the solid and liquid are of the same material. The volume of the solidified and liquid material may be constant or it may be permitted to increase at a specified rate. We only consider the solidification of pure elements or compounds with a single melting point. The liquid/gas interface and the solid/liquid interface are unknown coupled moving boundaries. The front at which the solid, liquid and gas meet is also a moving boundary to be determined. In the following six paragraphs, we discuss the assumptions concerning the solid, liquid and gas and their interfaces.

The solid is assumed to have the same thermal properties as the liquid. We model the solid as infinitely thick in comparison to the thin liquid film (discussed below). The solid is initially at a constant temperature lower than the liquid melting point, the far-field temperature remaining at this constant value.

The liquid is an incompressible fluid of constant viscosity. We approximate the density of the fluid to be the same (constant) value as the density of the solid. The modified Reynolds number and aspect ratio are taken to be small so that lubrication theory may be applied to simplify the Navier-Stokes equations. The equation for conservation of energy also greatly simplifies in this limit.

The gas is considered to be relatively passive. The gas is assumed to be maintained at a constant temperature which is lower than the liquid melting point. The gas, however, is a very poor conductor and the Biot number is not permitted to be large. This assumption is consistent with no solidification taking place at the liquid/gas interface.

Surface tension acts at the liquid/gas interface. Surface-tension effects are initially retained in the fluid model. The singular limit of large Bond number is adopted and, at this stage, surface-tension effects are neglected altogether. The liquid/gas interface may be oxidised, which would justify the neglect of surface tension for certain fluids. In this way, we avoid the specification of a contact-angle condition where solidification is taking place.

A Stefan condition is prescribed at the solid/liquid interface where solidification is expected to occur. Surface tension, undercooling and slip are ignored at the solid/liquid interface.

The propagation of two-dimensional and axisymmetric viscous gravity currents over a horizontal surface is susceptible to a fingering instability (see, for example, [7]). There are also stability issues related to the solid/liquid interface (see, for example, [8, Chapter 5]). Morphological instability is associated with supercooling of the fluid which is not considered here. In this article, we seek similarity solutions of the systems of partial differential equations; the stability of these solutions to perturbations is not discussed.

The purpose of this paper is to gain a better understanding of the flow of viscous gravity currents subject to thermal cooling and solidification. Mathematical models are introduced which take basal solidification into account. The fluid flow is dependent on the resolidified boundary through the geometry, this being a coupled moving-boundary problem. In the limiting cases of these models, analytical solutions are obtained which provide valuable insight.

The contents of the paper is now outlined. Based on the above assumptions, a new mathematical model is introduced in Section 2 and non-dimensionalised, enabling the dominant balances to be identified. The simplified two-dimensional and axisymmetric problems are

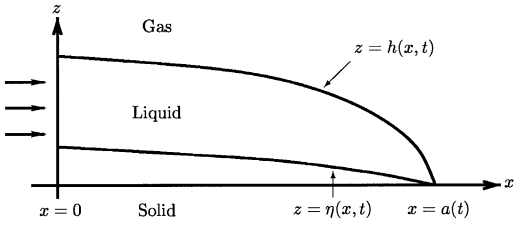

Figure 1. Planar representation of basal solidification. The horizontal direction is denoted by x and the vertical direction by z. The incompressible fluid is in the region $0 < x < a(t)$ and $\eta(x,t) < z < h(x,t)$, and the solid is in the region $z < \eta(x,t)$. The arrows at $x = 0$ denote inflow.

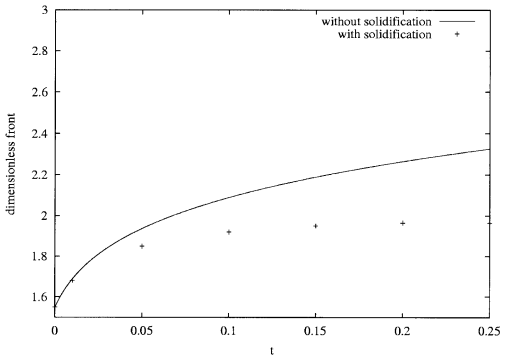

Figure 3. Front location as a function of time for the spreading of an axisymmentric drop of water with and without basal solidification in the parameter régime $B = 0, D \gg 1$ and $\lambda_f = O(D^{1/2})$. The arrest of the front motion takes place at a dimensionless time of $t \approx 0{\cdot}2$. The contact line is obtained from the leading-order balance in (34) subject to (41) and (51–52).

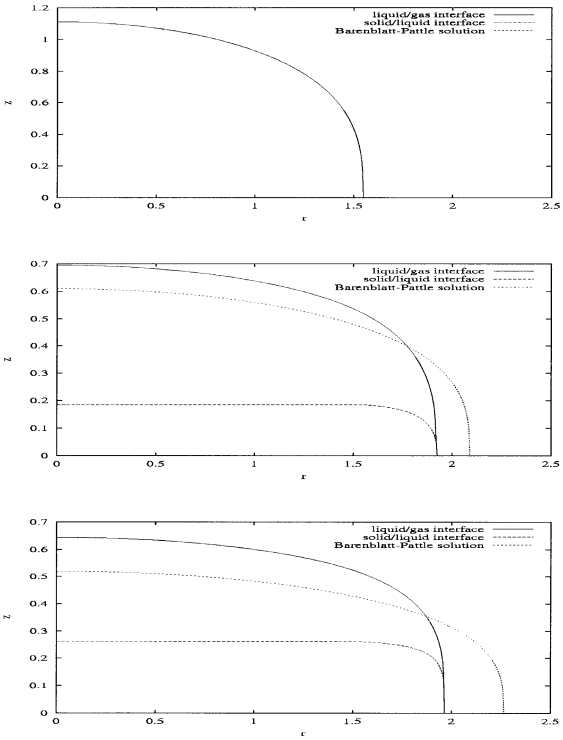

Figure 2. Spreading and solidification of an axisymmetric drop of water with $B = 0, D \gg 1$ and $\lambda_f = O(D^{1/2})$ at times $t = 0$ (top), $t = 0{\cdot}1$ (middle) and $t = 0{\cdot}2$ (bottom). The liquid/gas and solid/liquid interface are compared with the Barenblatt-Pattle similarity solution without solidification. The interfaces are obtained from the leading-order balance in (34) subject to (41) and (51–52).

derived in Section 3, the small parameters being the square of the aspect ratio, the modified Reynolds number and the reciprocal of the Bond number. The physical problem contains coupled moving boundaries, however, in the asymptotic limit, this reduces to an explicit equation for the free fluid surface with only the thermal equation remaining as a field equation. Section 4 describes three asymptotic solutions to the leading-order problem. In Section 5, results are presented for the spreading and basal solidification of two common laboratory solvents, namely water and glycerol. Finally, Section 6 gives a brief discussion of the results.

2. Problem formulation

2.1. Two-dimensional model

2.1.1. *Mathematical model*

We consider an incompressible fluid contained in the horizontal direction by $0 < x < a(t)$ and in the vertical direction by a bottom defined by $z = \eta(x,t)$ and a top defined by $z = h(x,t)$

as indicated in Figure 1, where x and z are the coordinates in the horizontal and vertical directions and t is time. Solidified material is present in the region $z < \eta(x,t)$. The initial-boundary-value problem for the horizontal velocity $u(x,z,t)$, vertical velocity $w(x,z,t)$, $(\boldsymbol{q} = (u,w)^T)$, pressure $p(x,z,t)$, temperature $T(x,z,t)$, the position of the front $x = a(t)$, the dynamic contact angle $\Theta(t)$, and unknown moving boundaries $z = \eta(x,t)$ and $z = h(x,t)$ is

$$\nabla \cdot \boldsymbol{q} = 0, \quad \rho\left[\frac{\partial \boldsymbol{q}}{\partial t} + (\boldsymbol{q}\cdot\nabla)\boldsymbol{q}\right] = -\nabla p + \mu\nabla^2\boldsymbol{q} - \rho g\boldsymbol{k} \quad \text{for} \quad \eta(x,t) < z < h(x,t), \tag{1}$$

$$\rho c\left[\frac{\partial T}{\partial t} + (\boldsymbol{q}\cdot\nabla)T\right] = k\nabla^2 T \quad \text{for} \quad \eta(x,t) < z < h(x,t), \tag{2}$$

$$\frac{\partial T}{\partial t} = \frac{k}{\rho c}\nabla^2 T \quad \text{for} \quad z < \eta(x,t), \tag{3}$$

$$\frac{\mathrm{D}}{\mathrm{D}t}(z-h) = 0, \quad \boldsymbol{n}\cdot\boldsymbol{\tau}\cdot\boldsymbol{n} = 2\kappa\sigma, \quad \boldsymbol{t}\cdot\boldsymbol{\tau}\cdot\boldsymbol{n} = 0 \quad \text{on} \quad z = h(x,t), \tag{4}$$

$$\gamma(T - T_a) = -k\nabla T\cdot\nabla(z-h) \quad \text{on} \quad z = h(x,t), \tag{5}$$

$$T = T_m, \quad \boldsymbol{q}\cdot\nabla(z-\eta) = 0, \quad \boldsymbol{t}\cdot\boldsymbol{q} = 0 \quad \text{on} \quad z = \eta(x,t), \tag{6}$$

$$\rho L_f\frac{\partial \eta}{\partial t} + [k\nabla T]_{\eta^-}^{\eta^+}\cdot\nabla(z-\eta) = 0 \quad \text{on} \quad z = \eta(x,t), \tag{7}$$

$$T \to T_a \quad \text{as} \quad z \to -\infty, \tag{8}$$

$$a(t) = \sup\{x : h(x,t) - \eta(x,t) > 0\}, \quad V(t) = \int_{x=0}^{a(t)} h(x,t)\mathrm{d}x, \tag{9}$$

$$\left(\frac{\partial \eta}{\partial x} - \frac{\partial h}{\partial x}\right)(a(t),t) = \tan(\Theta(t)), \tag{10}$$

where ρ is the density, μ the viscosity, g the acceleration due to gravity, $\boldsymbol{k} = (0,1)^T$, c the specific heat capacity, k the thermal conductivity, σ the surface tension, γ the heat-transfer coefficient, T_m the melting temperature, L_f the latent heat of fusion, $V(t)$ the prescribed volume per unit length, τ denotes the stress tensor of the liquid, $\boldsymbol{n}$ is the unit normal vector pointing out of the liquid, $\boldsymbol{t}$ is the unit tangential vector, T_a is the ambient temperature and the differential operator $\nabla = (\partial/\partial x, \partial/\partial z)$. The mean curvature κ is given by

$$2\kappa = \nabla\cdot\left([1 + |\nabla h|^2]^{-1/2}\nabla h\right).$$

We assume the melting point is above the ambient temperature, that is $T_m > T_a$. We will assume that the volume per unit length to be of the form $V(t) = qt^\alpha$ in two dimensions and the volume to be of the form $V(t) = Qt^\alpha$ in the axisymmetric case, where q and Q are constants.

Equations (1) and (2) describe the conservation of mass, momentum and energy in the liquid, while equation (3) represents conservation of energy in the solid. The first boundary condition in (4) and (5) are the conservation of mass and energy, while the second and third

in (4) balance the normal and tangential stress components across the liquid/gas interface. The boundary condition in (5) may break down near the front (when $h - \eta$ is smaller than the thickness of the thermal boundary layer in the gas), but for the purposes of this article, it is adopted as a reasonable approximation. The first boundary condition in (6) is the melting isotherm, the second conservation of mass and the third the no-slip condition. The issue of whether or not basal solidification relieves the stress singularity at the front is an interesting one. The no-slip condition is adopted until the requirement for slip has been established. Equation (7) denotes conservation of energy at the solid/liquid interface. Equation (8) describes the ambient temperature in the body of the solidified material. The first condition in (9) defines the front and the second relates to a global conservation of mass. Equation (10) introduces the dynamic contact angle. We do not prescribe any contact-angle condition in this model; this will be discussed below.

Anderson *et al.* [9] recently presented results concerning the contact angle in the presence of solidification. These results concern geometrical models in which the solidified boundary is assumed to be horizontal. Comparison between continuum models and experimental results is required before these theories may be considered valid approximations in general. We make no attempt to specify a contact-angle condition in this paper.

The system of Equations (1–10) is not only lacking in a contact-angle condition, but also a boundary condition at $x = 0$. In the case of a non-zero inflow (that is $\mathrm{d}V/\mathrm{d}t$ non-zero), it is necessary to consider a more sophisticated model of the inflow itself. In the zero inflow case, the line $x = 0$ may be considered as a line of symmetry and we require

$$\frac{\partial w}{\partial x} = 0.$$

the axisymmetric version of this condition is obtained by replacing x by r.

2.1.2. *Non-dimensionalisation*

We define a_0 and U to be typical values of the horizontal length-scale and velocity. A representative value of the small aspect ratio is denoted by δ. We transform to dimensionless variables via

$$x = a_0 x^*,\ z = \delta a_0 z^*,\ t = \frac{a_0}{U} t^*,\ u = U u^*,\ w = \delta U w^*,\ p = \frac{\mu U}{a_0 \delta^2} p^*,\ \Theta = \delta \Theta^*,$$

$$T = T_a + (T_m - T_a)T^*, \quad V = a_0^2 \delta V^*, \quad h = \delta a_0 h^*, \quad \eta = \delta a_0 \eta^*, a = a_0 a^*.$$

Conservation of mass in the liquid determines the vertical velocity scale. We note that the dominant flow direction is horizontal. The pressure scale is obtained by balancing pressure gradients and viscous terms in the horizontal component of the equation for conservation of momentum. The system of equations (1–10) then becomes (and without ambiguity the asterisks on the non-dimensional variables can be omitted):

$$\frac{\partial u}{\partial x} + \frac{\partial w}{\partial z} = 0,\ \mathrm{Re}\delta^2 \left[\frac{\partial u}{\partial t} + u\frac{\partial u}{\partial x} + w\frac{\partial u}{\partial z} \right] = -\frac{\partial p}{\partial x} + \delta^2 \frac{\partial^2 u}{\partial x^2} + \frac{\partial^2 u}{\partial z^2} \text{for } \eta(x,t) < z < h(x,t), \quad (11)$$

$$\mathrm{Re}\delta^4 \left[\frac{\partial w}{\partial t} + u\frac{\partial w}{\partial x} + w\frac{\partial w}{\partial z} \right] = -\frac{\partial p}{\partial z} + \delta^4 \frac{\partial^2 w}{\partial x^2} + \delta^2 \frac{\partial^2 w}{\partial z^2} - \frac{G}{C} \text{for } \eta(x,t) < z < h(x,t), \quad (12)$$

$$\frac{1}{D} \left[\frac{\partial T}{\partial t} + u\frac{\partial T}{\partial x} + w\frac{\partial T}{\partial z} \right] = \delta^2 \frac{\partial^2 T}{\partial x^2} + \frac{\partial^2 T}{\partial z^2} \quad \text{for } \eta(x,t) < z < h(x,t), \quad (13)$$

$$\frac{1}{D}\frac{\partial T}{\partial t} = \delta^2\frac{\partial^2 T}{\partial x^2} + \frac{\partial^2 T}{\partial z^2} \quad \text{for} \quad z < \eta(x,t), \tag{14}$$

$$w = \frac{\partial h}{\partial t} + u\frac{\partial h}{\partial x},\ p = -\frac{1}{C}\frac{\partial^2 h}{\partial x^2} + O(\delta^2),\ \frac{\partial u}{\partial z} = O(\delta^2),\ \frac{\partial T}{\partial z} + BT = O(\delta^2) \text{ on } z = h(x,t), \tag{15}$$

$$T = 1,\ \ w = u\frac{\partial \eta}{\partial x},\ \ u = O(\delta^2),\ \ \lambda_f\frac{\partial \eta}{\partial t} + D\left[\frac{\partial T}{\partial z} - \delta^2\frac{\partial \eta}{\partial x}\frac{\partial T}{\partial x}\right]_{\eta^-}^{\eta^+} = 0 \text{ on } z = \eta(x,t), \tag{16}$$

$$T \to 0 \quad \text{as} \quad z \to -\infty, \tag{17}$$

$$a(t) = \sup\{x : h(x,t) - \eta(x,t) > 0\}, \qquad V(t) = \int_{x=0}^{a(t)} h(x,t)\mathrm{d}x, \tag{18}$$

$$\left(\frac{\partial \eta}{\partial x} - \frac{\partial h}{\partial x}\right)(a(t),t) = \Theta(t) + O(\delta^2). \tag{19}$$

A number of dimensionless parameters arise, namely the Reynolds number Re, the Bond number G, the capillary number C, the Peclet number Pe, the Biot number B, the Stefan number for fusion λ_f and the reciprocal of the reduced Peclet number $D = 1/\mathrm{Pe}\delta^2$. We define these parameters as follows

$$\mathrm{Re} = \frac{\rho U a_0}{\mu}, \quad G = \frac{\rho g a_0^2}{\sigma}, \quad C = \frac{\mu U}{\sigma\delta^3},$$

$$\mathrm{Pe} = \frac{\rho c U a_0}{k}, \quad B = \frac{a_0\delta\gamma}{k}, \quad \lambda_f = \frac{L_f}{c(T_m - T_a)}.$$

We adopt the lubrication and large-Bond-number limit based on the assumptions of small aspect ratio squared ($\delta^2 \ll 1$), small modified Reynolds number ($\mathrm{Re}\delta^2 \ll 1$), the large Bond number ($G \gg 1$) and $G/C = O(1)$. The Bond number is a ratio of gravitational forces to surface tension. The lack of influence of the front on the overall behaviour at large Bond numbers is well-known (see [1]), this being the régime where we shall eventually seek solutions. We assume $D = O(1)$, $B = O(1)$ and $\lambda_f = O(1)$ until otherwise indicated.

2.2. Axisymmetric model

The same notation for velocity, pressure, temperature and the moving boundaries will be adopted for the axisymmetric model; these quantities are defined anew. We consider an incompressible fluid contained in the radial direction by $0 < r < a(t)$ and in the vertical direction by a bottom defined by $z = \eta(r,t)$ and a top defined by $z = h(r,t)$, where r and z are the coordinates in the radial and vertical directions and t is time (as shown in Figure 1 except that the radial coordinate r replaces x). Solidified material is present in the region $z < \eta(r,t)$. The axisymmetric version (see [10, p. 602]) of the initial-boundary-value problem (1–10) for the radial velocity $u(r,z,t)$, vertical velocity $w(r,z,t)$, pressure $p(r,z,t)$, temperature $T(r,z,t)$, the position of the front $r = a(t)$, the dynamic contact angle $\Theta(t)$ and unknown free surfaces $z = \eta(r,t)$ and $z = h(r,t)$ is transformed to dimensionless variables via

$$r = a_0 r^*, \quad z = \delta a_0 z^*, \quad t = \frac{a_0}{U}t^*, \quad u = Uu^*, \quad w = \delta U w^*, \quad p = \frac{\mu U}{a_0\delta^2}p^*, \quad \Theta = \delta\Theta^*,$$

$$T = T_a + (T_m - T_a)T^*, \quad V = 2\pi a_0^3 \delta V^*, \quad h = \delta a_0 h^*, \quad \eta = \delta a_0 \eta^*, \quad a = a_0 a^*,$$

where a_0 and U now represent typical values of the radial length-scale and velocity. The resulting system of equations is not stated here, the leading-order axisymmetric problem is summarised in Subsection 3.2.

3. Leading-order problem

3.1. Two-dimensional model

3.1.1. *Asymptotic analysis*

Equations (1–10) are formidable both from an analytical and numerical viewpoint. If predictions are to result, then a lubrication and large-Bond-number limit is desirable to make the equations tractable. We introduce expansions of the form

$$u \sim u_0, \quad w \sim w_0, \quad p \sim p_0, \quad T \sim T_0, \quad a \sim a_0, \quad \eta \sim \eta_0, \quad h \sim h_0,$$

as $\delta^2 \to 0$, $\mathrm{Re}\delta^2 \to 0$, $1/G \to 0$ and define $\Lambda = G/C = O(1)$. Hocking [2] found that the large-Bond-number problem split into three asymptotic regions in the absence of solidification, namely an outer solution where gravity dominates capillarity, an intermediate region where capillarity and gravity are of equal importance and an inner region where capillarity is dominant but slip can no longer be ignored. This analysis justifies the use of the outer solution as a reasonable approximation to the whole solution; the approach having been shown to produce satisfactory agreement with experiment in predicting the overall shape [1]. Henceforth, we shall adopt the outer solution accepting that the liquid/gas interface we obtain will have an unphysical vertical gradient in the neighbourhood of the front. The analysis in [2] also shows that this approximation becomes invalid when the time-scale of spreading is large; the analysis which follows will be applicable while viscosity, gravity and basal solidification remain dominant.

Integrating the equation for conservation of mass (the first equation in (11)) across the fluid layer and using the conservation of mass boundary conditions at the liquid/gas interface (the first in (15)) and the solid/liquid interface (the second in (16)), we obtain

$$\frac{\partial h_0}{\partial t} + \frac{\partial}{\partial x} \int_{z=\eta_0}^{z=h_0} u_0 \mathrm{d}z = 0. \tag{20}$$

The integration of the leading-order balance between pressure gradient and hydrostatic forces in (12) and application of the normal stress boundary condition (the second in (15)) gives

$$p_0 = \Lambda(h_0 - z).$$

Now the second equation in (11) is integrated three times with respect to z with the tangential-stress condition (the third in (15)) and no-slip condition (the third in (16)), to obtain

$$\int_{z=\eta_0}^{z=h_0} u_0 \mathrm{d}z = -\frac{\Lambda}{3} \frac{\partial h_0}{\partial x} (h_0 - \eta_0)^3. \tag{21}$$

Equations (20) and (21) give the evolution equation for the free surface $h_0(x, t)$, that is,

$$\frac{\partial h_0}{\partial t} + \frac{\partial}{\partial x} \left[-\frac{\Lambda}{3} \frac{\partial h_0}{\partial x} (h_0 - \eta_0)^3 \right] = 0. \tag{22}$$

The horizontal velocity is then known in terms of the two free boundaries η_0 and h_0, we have

$$u_0 = -\frac{\Lambda}{2}\frac{\partial h_0}{\partial x}(z-\eta_0)(2h_0 - z - \eta_0). \tag{23}$$

By use of the first equation in (11) and the second condition in (16), the vertical velocity may be obtained

$$w_0 = -\frac{\Lambda}{6}\frac{\partial^2 h_0}{\partial x^2}(\eta_0 - z)^2(2\eta_0 - 3h_0 + z) - \Lambda\frac{\partial h_0}{\partial x}(z-\eta_0)\left(-\frac{1}{2}\frac{\partial h_0}{\partial x}(z-\eta_0) + \frac{\partial \eta_0}{\partial x}(h_0 - \eta_0)\right). \tag{24}$$

3.1.2. *Summary of the two-dimensional problem* $\delta^2 \ll 1$, $\mathrm{Re}\delta^2 \ll 1$, $G \gg 1$, $\Lambda = O(1)$
We summarise the two-dimensional model in conservative form (which is more suitable for numerical solution) to describe the coupling of gravity, viscosity and basal solidification. The subscripts on the leading-order terms will be omitted without ambiguity. The leading-order equations in the fluid are given by

$$\frac{\partial}{\partial t}(h-\eta) + \frac{\partial}{\partial x}\left[-\frac{\Lambda}{3}\frac{\partial h}{\partial x}(h-\eta)^3\right] = -\frac{\partial \eta}{\partial t}, \tag{25}$$

$$\frac{\partial T}{\partial t} + \frac{\partial}{\partial x}(uT) + \frac{\partial}{\partial z}(wT) = D\frac{\partial^2 T}{\partial z^2}, \tag{26}$$

$$u = -\frac{\Lambda}{2}\frac{\partial h}{\partial x}(z-\eta)(2h - z - \eta), \tag{27}$$

$$w = -\frac{\Lambda}{6}\frac{\partial^2 h}{\partial x^2}(\eta - z)^2(2\eta - 3h + z) - \Lambda\frac{\partial h}{\partial x}(z-\eta)\left(-\frac{1}{2}\frac{\partial h}{\partial x}(z-\eta) + \frac{\partial \eta}{\partial x}(h-\eta)\right), \tag{28}$$

at the liquid/gas interface,

$$\text{on} \quad z = h \quad \frac{\partial T}{\partial z} + BT = 0, \tag{29}$$

at the solid/liquid interface,

$$\lambda_f\frac{\partial \eta}{\partial t} + D\left[\frac{\partial T}{\partial z}\right]_{\eta^-}^{\eta^+} = 0, \qquad \text{on } z = \eta \quad T = 1, \tag{30}$$

in the solid,

$$\frac{\partial T}{\partial t} = D\frac{\partial^2 T}{\partial z^2} \quad \text{for } z < \eta, \qquad T \to 0 \quad \text{as } z \to -\infty, \tag{31}$$

and at the front,

$$a(t) = \sup\{x : h(x,t) - \eta(x,t) > 0\}, \qquad V(t) = \int_{x=0}^{a(t)} h(x,t)\mathrm{d}x. \tag{32}$$

The initial conditions are

$$h(x,0) = \bar{h}(x), \quad T(x,z,0) = \bar{T}(x,z), \quad \eta(x,0) = 0, \quad a(0) = \bar{a}, \quad V(0) = \bar{V}, \tag{33}$$

where we assume $\bar{T}(x,z) = 0$ for $z < 0$, $\bar{T}(x,0) = 1$, $\partial\bar{T}/\partial z(x,\bar{h}(x)) + B\bar{T}(x,\bar{h}(x)) = 0$ for $x < \bar{a}$, $\bar{T}(x,z) \geq 1$ for $0 < z \leq \bar{h}(x)$, $\bar{h}(\bar{a}) = 0$ and $\bar{V} = \int_{x=0}^{\bar{a}} \bar{h}(x)\mathrm{d}x$. The initial temperature of the solid is assumed to be ambient whereas the initial temperature of the fluid is at melting point at the solid/liquid interface, there being a discontinuous spatial derivative at $z = 0$. The four physical time-scales associated with fluid spreading, thermal convection, thermal conduction and basal solidification are given by

$$\frac{\mu}{\rho g \delta^3 a_0}, \quad \frac{a_0}{U}, \quad \frac{\rho c \delta^2 a_0^2}{k}, \quad \frac{\rho c \delta^2 a_0^2 \lambda_f}{k},$$

respectively. The conventional form of the lubrication equation has been modified by terms which relate to the solid/liquid interface, the term on the right-hand side of (25) representing the loss of mass due to basal solidification. We note that (25) is a degenerate parabolic partial differential equation. Equations (25) and (27–28) were previously obtained by Bunk [5]. This model is closed; it has the full complement of boundary conditions.

3.2. Summary of the axisymmetric problem: $\delta^2 \ll 1$, $\mathrm{Re}\delta^2 \ll 1$, $G \gg 1$, $\Lambda = O(1)$

The analysis in the axisymmetric case is similar to the two-dimensional case (see Subsection 3.1.1) and only the result will be outlined below. We summarise the axisymmetric model in conservative form which describes the coupling of gravity, viscosity and basal solidification. The subscripts on the leading-order terms will be omitted without ambiguity. The leading-order equations in the fluid are

$$\frac{\partial}{\partial t}(h-\eta) + \frac{1}{r}\frac{\partial}{\partial r}\left[-r\frac{\Lambda}{3}\frac{\partial h}{\partial r}(h-\eta)^3\right] = -\frac{\partial \eta}{\partial t}, \tag{34}$$

$$\frac{\partial T}{\partial t} + \frac{1}{r}\frac{\partial}{\partial r}(ruT) + \frac{\partial}{\partial z}(wT) = D\frac{\partial^2 T}{\partial z^2}, \tag{35}$$

$$u = -\frac{\Lambda}{2}\frac{\partial h}{\partial r}(z-\eta)(2h-z-\eta), \tag{36}$$

$$w = -\frac{\Lambda}{6r}\frac{\partial}{\partial r}\left(r\frac{\partial h}{\partial r}\right)(\eta-z)^2(2\eta-3h+z) - \Lambda\frac{\partial h}{\partial r}(z-\eta)\left(-\frac{1}{2}\frac{\partial h}{\partial r}(z-\eta) + \frac{\partial \eta}{\partial r}(h-\eta)\right), \tag{37}$$

at the liquid/gas interface,

$$\text{on} \quad z = h \qquad \frac{\partial T}{\partial z} + BT = 0, \tag{38}$$

at the solid/liquid interface,

$$\lambda_f \frac{\partial \eta}{\partial t} + D\left[\frac{\partial T}{\partial z}\right]_{\eta^-}^{\eta^+} = 0, \qquad \text{on} \quad z = \eta \quad T = 1, \tag{39}$$

in the solid,

$$\frac{\partial T}{\partial t} = D\frac{\partial^2 T}{\partial z^2} \quad \text{for } z < \eta, \qquad T \to 0 \quad \text{as} \quad z \to -\infty, \tag{40}$$

and at the front

$$a(t) = \sup\{r : h(r,t) - \eta(r,t) > 0\}, \qquad V(t) = \int_{r=0}^{a(t)} h(r,t) r \mathrm{d}r. \tag{41}$$

The initial conditions are

$$h(r,0) = \bar{h}(r), \quad T(r,z,0) = \bar{T}(r,z), \quad \eta(r,0) = 0, \quad a(0) = \bar{a}, \quad V(0) = \bar{V}, \tag{42}$$

where we assume $\bar{T}(r,z) = 0$ for $z < 0$, $\bar{T}(r,0) = 1$, $\partial\bar{T}/\partial z(r,\bar{h}(r)) + B\bar{T}(r,\bar{h}(r)) = 0$ for $r < \bar{a}$, $\bar{T}(r,z) \geq 1$ for $0 < z \leq \bar{h}(r)$, $\bar{h}(\bar{a}) = 0$ and $\bar{V} = \int_{r=0}^{\bar{a}} \bar{h}(r) r \mathrm{d}r$. Similar comments to those in Subsection 3.1.2 concerning (25–33) may now be applied to (34–42).

4. Analytical solutions

4.1. The intermediate time-scale similarity transformation

4.1.1. *Introduction*

In the absence of basal solidification, Huppert [1] described a family of similarity solutions for two-dimensional (axisymmetric) viscous gravity currents where the volume per unit length is of the form $V = qt^{\alpha}$ (volume is of the form $V = Qt^{\alpha}$) and $\alpha < 7/4 (\alpha < 3)$. The inclusion of the basal solidification modifies the structure of the equations. In general, the large-time motion of the front is no longer given by $a(t) \sim t^{(3\alpha+1)/5}$ ($a(t) \sim t^{(3\alpha+1)/8}$) for the two-dimensional (axisymmetric) problem; the required continuous symmetry group is not available. The front motion is complicated by basal solidification modifying the flow at leading order (see Section 5). Two exceptional cases are described below in Subsections 4.1.2 and 4.1.3.

4.1.2. *The $B = 0$, $V \propto t^{7/4}$, large Julian number two-dimensional problem*

The $V \propto t^{7/4}$ and large-Julian-number régime corresponds to the limit where inertial effects are insignificant in comparison to viscous effects for all time [1], where the Julian number is given by $\nu^3 g^2/q^4$ and $\nu = \mu/\rho$ is the kinematic viscosity. In the absence of basal solidification, the energy equation decouples and the solution is self-similar with

$$u = t^{1/4} u^{\dagger}(\zeta,\xi), \quad w = t^{-1/2} w^{\dagger}(\zeta,\xi), \quad h = t^{1/2} h^{\dagger}(\zeta), \quad a = t^{5/4} a^{\dagger}, \quad V = t^{7/4} V^{\dagger},$$

in which $\zeta = x/t^{5/4}$ and $\xi = z/t^{1/2}$. This similarity transformation has been reported in [1]. In this subsection we consider how to generalise this result to include basal solidification.

We consider time-scales such that the conduction length-scale is much larger than the vertical dimension of the fluid drop. Therefore the detailed structure of the initial condition for temperature will have smoothed under the action of conduction. The fluid layer is assumed to be deep enough that solidification does not engulf the flow at any point. We therefore consider an intermediate time-scale and length-scale when this nonlinear system has a self-similar solution with

$$T = T^{\dagger}(\zeta,\xi), u = t^{1/4} u^{\dagger}(\zeta,\xi), w = t^{-1/2} w^{\dagger}(\zeta,\xi), \eta = t^{1/2}\eta^{\dagger}(\zeta),$$
$$h = t^{1/2} h^{\dagger}(\zeta), a = t^{5/4} a^{\dagger}, V = t^{7/4} V^{\dagger}.$$

Equations (25–32) transform to

$$\frac{h^\dagger}{2} - \frac{5\zeta}{4}\frac{\mathrm{d}h^\dagger}{\mathrm{d}\zeta} - \frac{\Lambda}{3}\frac{\mathrm{d}}{\mathrm{d}\zeta}\left[\frac{\mathrm{d}h^\dagger}{\mathrm{d}\zeta}(h^\dagger - \eta^\dagger)^3\right] = 0, \tag{43}$$

$$-\frac{5\zeta}{4}\frac{\partial T^\dagger}{\partial \zeta} - \frac{\xi}{2}\frac{\partial T^\dagger}{\partial \xi} + \frac{\partial}{\partial \zeta}(u^\dagger T^\dagger) + \frac{\partial}{\partial \xi}(w^\dagger T^\dagger) = D\frac{\partial^2 T^\dagger}{\partial \xi^2} \quad \text{for} \quad \eta^\dagger < \xi < h^\dagger, \tag{44}$$

$$u^\dagger = -\frac{\Lambda}{2}\frac{\mathrm{d}h^\dagger}{\mathrm{d}\zeta}(\xi - \eta^\dagger)(2h^\dagger - \xi - \eta^\dagger), \tag{45}$$

$$w^\dagger = -\frac{\Lambda}{6}\frac{\mathrm{d}^2 h^\dagger}{\mathrm{d}\zeta^2}(\eta^\dagger - \xi)^2(2\eta^\dagger - 3h^\dagger + \xi) - \Lambda\frac{\mathrm{d}h^\dagger}{\mathrm{d}\zeta}(\eta^\dagger - \xi)\left(\frac{1}{2}\frac{\mathrm{d}h^\dagger}{\mathrm{d}\zeta}(\eta^\dagger - \xi) + \frac{\mathrm{d}\eta^\dagger}{\mathrm{d}\zeta}(h^\dagger - \eta^\dagger)\right), \tag{46}$$

$$\lambda_f\left(\frac{\eta^\dagger}{2} - \frac{5\zeta}{4}\frac{\mathrm{d}\eta^\dagger}{\mathrm{d}\zeta}\right) + D\left[\frac{\partial T^\dagger}{\partial \xi}\right]_{\eta^{\dagger-}}^{\eta^{\dagger+}} = 0 \quad \text{on } \xi = \eta^\dagger \; T^\dagger = 1, \tag{47}$$

$$-\frac{5\zeta}{4}\frac{\partial T^\dagger}{\partial \zeta} - \frac{\xi}{2}\frac{\partial T^\dagger}{\partial \xi} = D\frac{\partial^2 T^\dagger}{\partial \xi^2} \qquad \text{for} \quad \xi < \eta^\dagger, \quad \text{as } \xi \to -\infty \; T^\dagger \to 0, \tag{48}$$

for $0 < \zeta < a^\dagger$ and

$$h^\dagger(a^\dagger) = \eta^\dagger(a^\dagger), \qquad V^\dagger = \int_{\zeta=0}^{a^\dagger} h^\dagger \mathrm{d}\zeta. \tag{49}$$

The Equations (43–46) and (49) have already been derived by Bunk [5]. Bunk did not include latent heat or heat conduction in the solid, so Equations (47–48) are introduced here. The front has the same time dependence with basal solidification as it does without [1]. The effect of solidification is to modify the system of equations satisfied by the constant of proportionality $a^\dagger$. We anticipate that $a^\dagger$ will be smaller with basal solidification than without. However, it does not appear possible to deduce this result analytically from (43–49).

4.1.3. *The $B = 0$, $V \propto t^3$, $\nu g/Q \gg 1$ axisymmetric problem*

This régime corresponds to the limit where inertial effects are insignificant in comparison to viscous effects for all time in the axisymmetric case [1]. In the absence of basal solidification, a self-similar solution

$$u = t^{1/4}u^\ddagger(\zeta, \xi),\ w = t^{-1/2}w^\ddagger(\zeta, \xi),\ h = t^{1/2}h^\ddagger(\zeta),\ a = t^{5/4}a^\ddagger,\ V = t^3 V^\ddagger,$$

where $\zeta = r/t^{5/4}$ and $\zeta z = z/t^{1/2}$ has been reported in [1]. We consider an intermediate time-scale and length-scale, as argued in Subsection 4.1.2, when the solution of the nonlinear system (34–41) has a self-similar solution with

$$T = T^\ddagger(\zeta, \xi),\ u = t^{1/4}u^\ddagger(\zeta, \xi),\ w = t^{-1/2}w^\ddagger(\zeta, \xi),\ \eta = t^{1/2}\eta^\ddagger(\zeta),$$

$$h = t^{1/2}h^\ddagger(\zeta),\ a = t^{5/4}a^\ddagger,\ V = t^3 V^\ddagger.$$

Equations (34–41) transform to a similar system to (43–49). We observe, as in Subsection 4.1.2, that the front has the same time dependence with basal solidification as it does without. The effect of solidification is to modify the system of equations satisfied by the constant of proportionality $a^\ddagger$.

4.2. THE $B = 0$, $D \gg 1$ AND $\lambda_f = O(D^{1/2})$ TWO-DIMENSIONAL (AXISYMMETRIC) PROBLEM

We consider the liquid/gas interface to be adiabatic ($B = 0$), small modified Peclet number ($D \gg 1$) and large latent heat of fusion ($\lambda_f = O(D^{1/2})$). We note that if we had adopted $\lambda_f = O(1)$ the liquid would solidify without any significant spreading. Therefore, we take the latent heat of fusion to be large in comparison to sensible heat. In the following we also assume $D\delta^2 \ll 1$ so that the lateral thermal conduction terms remain negligible. The two-dimensional model (25–32) and the axisymmetric model (34–41) are singularly perturbed in the small parameter $1/D$, there being an initial inner expansion for $t = O(1/D)$. A similar limit was previously adopted in [3] (see the Appendix) and [11], however, the inner expansion was not considered.

4.2.1. *Inner expansion: $t = O(1/D)$*

In this inner expansion the appropriate scalings are (with no ambiguity with the earlier derivation of the lubrication and large-Bond-number limit)

$$t = t_1/D, \quad T \sim T_0, \quad \eta \sim \frac{1}{\lambda_f}\eta_0, \quad h \sim \bar{h},$$

as $1/\lambda_f \to 0$ and $1/D \to 0$ corresponding to a rapid change in temperature and small changes in the moving boundaries. The leading-order temperature in the fluid is given by

$$T_0 = 1 + \sum_{n=0}^{\infty} A_n \exp\left(-\frac{(2n+1)^2\pi^2 t_1}{4\bar{h}^2}\right) \sin\left(\frac{(2n+1)\pi z}{2\bar{h}}\right),$$

where the coefficients $A_n(x)(A_n(r)$ in the axisymmetric case) are obtained from the initial conditions

$$A_n = \frac{2}{\bar{h}} \int_{z=0}^{\bar{h}} \left(\bar{T} - 1\right) \sin\left(\frac{(2n+1)\pi z}{2\bar{h}}\right) \mathrm{d}z.$$

The thermal problem in the solid is self-similar with solution

$$T_0 = 1 + \mathrm{erf}\left(\frac{z}{2t_1^{1/2}}\right).$$

The position of the solid/liquid interface may now be deduced from the first equation in (30) (the first equation in (39) for the axisymmetric case)

$$\eta_0 = 2\sqrt{\frac{t_1}{\pi}} + \sum_{n=0}^{\infty} \frac{2\bar{h}A_n}{(2n+1)\pi} \left[\exp\left(-\frac{(2n+1)^2\pi^2 t_1}{4\bar{h}^2}\right) - 1\right].$$

The derivative $\partial\eta_0/\partial t_1$ is singular at $t_1 = 0$, but there is no new balance in the equations and no additional expansion is required.

4.2.2. *Outer expansion: $t = O(1)$*

The leading-order temperature in the fluid has now reached a pseudo steady state, but the moving boundaries now vary at leading order. Here we require $D^{1/2}/\lambda_f = \Upsilon = O(1)$ to achieve order one variation in the solidification. The appropriate scalings are (with no ambiguity with the earlier derivation of the lubrication and large-Bond-number limit)

$$T \sim T_0, \quad \eta \sim \eta_0, \quad h \sim h_0, \quad a \sim a_0,$$

as $1/\lambda_f \to 0$ and $1/D \to 0$. The temperature in the fluid is at the melting point $T_0 = 1$ whereas in the solid it is necessary to rescale $z = D^{1/2}y$ to retain the leading-order balance, we have

$$T_0 = 1 + \operatorname{erf}\left(\frac{y}{2t^{1/2}}\right). \tag{50}$$

The solid/liquid interface is determined by the removal of heat generated by the phase change. The temperature gradients have become much smaller on this longer time-scale. We integrate the first equation in (30) (the first equation in (39) for the axisymmetric case) and match with the inner expansion to obtain

$$\eta_0(x,t) = 2\Upsilon\sqrt{\frac{t}{\pi}} \qquad \left(\eta_0(r,t) = 2\Upsilon\sqrt{\frac{t}{\pi}}\right), \tag{51}$$

where $x < \bar{a}(r < \bar{a})$ and $\eta_0 < h_0$. The solidification is initiated at a time $\hat{t}$ when the front first reaches a location, $\hat{t}(x)(\hat{t}(r))$ being the solution of the equation $x = a_0(\hat{t})(r = a_0(\hat{t}))$. If $\bar{a} < x < a_0(\bar{a} < r < a_0)$, then

$$\eta_0(x,t) = 2\Upsilon\sqrt{\frac{t-\hat{t}}{\pi}} \qquad \left(\eta_0(r,t) = 2\Upsilon\sqrt{\frac{t-\hat{t}}{\pi}}\right), \tag{52}$$

where $t > \hat{t}$.

The liquid/gas interface must be obtained numerically. The procedure on each time-step is now outlined. The leading-order balance in the nonlinear partial differential equation (25) ((34) in the axisymmetric case) is solved with a conventional numerical technique subject to the conditions (32) ((41) in the axisymmetric case) to obtain the liquid/gas interface and the function $a_0(t)$. The function $\hat{t}(x)(\hat{t}(r))$ is then updated. Finally, the solid/liquid interface is evaluated using the equations (51) and (52).

The analysis in this subsection is illustrated by considering an example of the spreading of water on ice in Section 5.

4.3. THE $V(t) = \bar{V}$ AND $D \ll 1$ PROBLEM

4.3.1. *Two-dimensional model*

Inner expansion: $t = O(1)$. We now consider the situation with constant volume per unit length ($V(t) = \bar{V}$) and large modified Peclet number ($D \ll 1$). The model is singularly perturbed in the small parameter D. In this case the solidified material has no effect on the leading-order problem for the fluid flow. However, the fluid flow affects the solidification through the front position. This allows well-known similarity solutions to be combined to form an analytical solution. We introduce expansions of the form

$$h \sim h_0, \quad T \sim T_0, \quad u \sim u_0, \quad w \sim w_0, \quad \eta \sim D^{1/2}\eta_0, \quad a \sim a_0,$$

as $D \to 0$.

We note that the above scalings represent the outer expansion in a singular perturbation in space. The inner region in the neighbourhood of the front corresponds to the scalings

$$h \sim D^{1/2}h_0, T \sim T_0, u \sim D^{3/4}u_0, w \sim D^{1/2}w_0,$$

$$\eta \sim D^{1/2}\eta_0, a \sim a_0, z = D^{1/2}Z, x = a_0(t) + D^{3/4}X.$$

We will ignore this region, just as in the large-Bond-number limit, assuming that this corresponds to an $O(D^{3/4})$ error in the location of the front and the outer expansion is a reasonable approximation to the solution except in the neighbourhood of the front.

The leading-order liquid/gas interface satisfies the equation

$$\frac{\partial h_0}{\partial t} + \frac{\partial}{\partial x}\left[-\frac{\Lambda}{3}h_0^3\frac{\partial h_0}{\partial x}\right] = 0,$$

with boundary condition $h_0(a_0(t), t) = 0$ and $\int_0^{a_0(t)} h_0(x, t)\mathrm{d}x = \bar{V}$. This is the simplest case of the two-dimensional problem studied in [1]. The solution is of the form

$$h_0 = \hat{a}^{2/3}\left(\frac{3\bar{V}^2}{\Lambda}\right)^{1/5} t^{-1/5}\phi\left(\frac{\xi}{\hat{a}}\right), \qquad \xi = \left(\frac{1}{3}\Lambda\bar{V}^3\right)^{-1/5} xt^{-1/5},$$

where $\hat{a}$ is the value of ξ at $x = a_0(t)$. We obtain the Barenblatt-Pattle solution

$$\phi(y) = \left(\frac{3}{10}\right)^{1/3}(1 - y^2)^{1/3}, \quad y = \frac{\xi}{\hat{a}}, \quad \hat{a} = \left[\frac{1}{5}\left(\frac{3}{10}\right)^{1/3}\frac{\pi^{1/2}\Gamma(1/3)}{\Gamma(5/6)}\right]^{-3/5}.$$

The leading-order velocities are now given by substitution of this expression for h_0 in (27) and (28). The leading-order temperature in the fluid is determined by the hyperbolic equation

$$\frac{\partial T_0}{\partial t} + u_0\frac{\partial T_0}{\partial x} + w_0\frac{\partial T_0}{\partial z} = 0,$$

such that T_0 is constant along the bicharacteristics $\mathrm{d}x/\mathrm{d}t = u_0$ and $\mathrm{d}z/\mathrm{d}t = w_0$. There is no boundary layer at $z = 0$ or $z = h_0$ in the fluid despite the removal of the highest derivative in the leading-order problem. (We note that if we had taken $B \gg 1$ then there would have been a thermal boundary layer at $z = h$. A new moving boundary must be incorporated to model any solidification in the form of a carapace.) In the solid there is an outer expansion and an inner expansion near $z = \eta$. The outer expansion in space is $T_0 \equiv 0$. We perform the stretching transformation $z = D^{1/2}Z$ in the boundary layer adjacent to the solid/liquid interface, to obtain the leading-order problem

$$\frac{\partial T_0}{\partial t} = \frac{\partial^2 T_0}{\partial Z^2},$$

with the boundary conditions

$$\lambda_f\frac{\partial \eta_0}{\partial t} = \frac{\partial T_0}{\partial Z}(x, \eta_0^-, t), \quad T_0(x, \eta_0, t) = 1, \quad T_0 \to 0 \text{ as } Z \to -\infty,$$

for $t > \hat{t}$ and the initial condition

$$T_0(x, Z, \hat{t}) = 0,$$

where $\hat{t} = 3(x/\hat{a})^5/(\Lambda\bar{V}^3)$. We thus obtain the Neumann solution

$$T_0 = \frac{1}{1+\text{erf}(\hat{\eta}/2)}\left(1+\text{erf}\left(\frac{Z}{2\sqrt{t-\hat{t}}}\right)\right), \quad \eta_0 = \hat{\eta}\sqrt{t-\hat{t}}, \tag{53}$$

for $t > \hat{t}$ where $\hat{\eta}$, is the unique root of the transcendental equation

$$\lambda_f \sqrt{\pi}\hat{\eta}\exp\left(\frac{\hat{\eta}^2}{4}\right)\left(1+\text{erf}\left(\frac{\hat{\eta}}{2}\right)\right) = 2. \tag{54}$$

The temperature in the fluid does not influence the leading-order term for solidification due to the absence of large temperature gradients. We note that the time derivative of the solidified boundary η_0 becomes singular as $t \to 0^+$, but this does not produce a new leading-order balance and there is no requirement for an additional inner time layer. This solution on $t = O(1)$ is an inner solution which breaks down on the longer time-scale $t = O(D^{-5/7})$.

Outer expansion: $t = O(D^{-5/7})$. On this time-scale, the basal solidification will engulf the flow. A number of variables need to be rescaled in this outer region, that is

$$t = D^{-5/7}\tilde{t}, \quad x = D^{-1/7}\tilde{x}, \quad z = D^{1/7}\tilde{z}, \quad u = D^{4/7}\tilde{u},$$
$$w = D^{6/7}\tilde{w}, \quad a = D^{-1/7}\tilde{a}, \quad h = D^{1/7}\tilde{h}, \quad \eta = D^{1/7}\tilde{\eta}.$$

The leading-order problem on this longer time-scale corresponds to a complete balance and no further analytical progress is possible. We note that for a two-dimensional drop of constant volume per unit length and poor conductivity, the final thickness of the resolidified material is $O(D^{1/7})$ spread over a region $O(D^{-1/7})$.

Bunk [5] concludes that latent heat release is of minor importance for large Prandtl number melts (or equivalently large Peclet number melts if $\text{Re} = O(1)$). This is true on the short time-scale because the solidification is small in comparison to the fluid depth. Latent heat is playing a minor role. However, he did not consider this long time-scale in which the fluid depth and solidification are of the same order. Here latent heat is present in the leading-order problem and plays a major role in controlling the fluid flow.

4.3.2. *Axisymmetric model*

Inner expansion: $t = O(1)$. The analysis is similar to the two-dimensional case and only the solution is summarised below. We introduce expansions of the form

$$h \sim h_0, \quad T \sim T_0, \quad u \sim u_0, \quad w \sim w_0, \quad \eta \sim D^{1/2}\eta_0, \quad a \sim a_0$$

as $D \to 0$. The solution is of the form

$$h_0 = \hat{a}^{2/3}\left(\frac{3\bar{V}}{\Lambda}\right)^{1/4} t^{-1/4}\psi\left(\frac{\xi}{\hat{a}}\right), \quad \xi = \left(\frac{1}{3}\Lambda\bar{V}^3\right)^{-1/8} r t^{-1/8}, \tag{55}$$

where $\hat{a}$ is the value of ξ at $x = a_0(t)$. We obtain the Barenblatt-Pattle solution

$$\psi(y) = \left(\frac{3}{16}\right)^{1/3}(1-y^2)^{1/3}, \quad y = \frac{\xi}{\hat{a}}, \quad \hat{a} = \left[\frac{2^{13}}{3^4}\right]^{1/8}.$$

The leading-order velocities are now given by substitution of this expression for h_0 in (36) and (37). The leading-order temperature in the fluid is determined by the hyperbolic equation

$$\frac{\partial T_0}{\partial t} + u_0\frac{\partial T_0}{\partial r} + w_0\frac{\partial T_0}{\partial z} = 0,$$

such that T_0 is constant along the bicharacteristics $\mathrm{d}r/\mathrm{d}t = u_0$ and $\mathrm{d}z/\mathrm{d}t = w_0$. In the solid there is an outer expansion and an inner expansion near $z = \eta$. The outer expansion is $T_0 \equiv 0$ and for the inner expansion, we recover (53–54) except that $\hat{t} = 3(r/\hat{a})^8/(\Lambda \overline{V}^3)$.

Outer expansion: $t = O(D^{-2/3})$. On this time-scale, the basal solidification will engulf the flow. A number of variables need to be rescaled in this outer region, that is

$$t = D^{-2/3}\tilde{t}, \quad r = D^{-1/12}\tilde{r}, \quad z = D^{1/6}\tilde{z}, \quad u = D^{7/12}\tilde{u},$$
$$w = D^{5/6}\tilde{w}, \quad a = D^{-1/12}\tilde{a}, \quad h = D^{1/6}\tilde{h}, \quad \eta = D^{1/6}\tilde{\eta}.$$

We note that for an axisymmetric drop of constant volume and poor conductivity, the final thickness of the resolidified material is $O(D^{1/6})$ spread over a region $O(D^{-1/12})$.

The analysis in this subsection is illustrated by considering an example of the spreading of liquid glycerol on solid glycerol in Section 5.

5. Results

5.1. Solidification of water

We now consider the spreading and basal solidification of an axisymmetric drop of water on a horizontal plane of ice. If we take the physical properties of water to be

$$\rho \sim 10^3 \text{ kgm}^{-3}, \quad c \sim 4 \times 10^3 \text{ Jkg}^{-1} \text{ K}^{-1}, \quad k \sim 0{\cdot}6 \text{ Js}^{-1} \text{ m}^{-1} \text{ K}^{-1},$$
$$\sigma \sim 8 \times 10^{-2} \text{ Nm}^{-1}, \quad \mu \sim 10^{-3} \text{ Nm}^{-2} \text{ s}, \quad L_f \sim 3 \times 10^5 \text{ Jkg}^{-1}, \quad T_m \sim 273 \text{ K},$$

(see, for example, [12]) along with the scales of the initial conditions

$$a_0 \sim 10^{-1} \text{ m}, \quad U \sim 10^{-3} \text{ ms}^{-1}, \quad \delta \sim 10^{-2}, \quad T_m - T_a \sim 10 \text{ K},$$

then we obtain

$$\mathrm{Re}\delta^2 \sim 10^{-2}, \quad C \sim 10, \quad G \sim 10^3, \quad \mathrm{Pe} \sim 10^3, \quad D \sim 10, \quad \lambda_f \sim 10.$$

These dimensionless constants are consistent with the assumptions adopted in Subsection 4.2. We note that, even though $\Lambda \sim 10^2$, it does not change the leading-order balance. The analysis of Subsection 4.2 will now be applied.

The evolution of the liquid/gas and solid/liquid interfaces of an axisymmetric drop is shown in Figure 2. The initial condition is taken to be consistent with the Barenblatt-Pattle solution (Subsection 4.3) and the free surfaces are compared with the Barenblatt-Pattle solution without solidification at subsequent times. The front is significantly retarded by the basal solidification. There is a critical time at which the radial spreading is arrested completely (shown in Figure 3). The instantaneous streamlines shown in Figure 4 correspond to the liquid/gas and solid/liquid interfaces in Figure 2. The velocity is decreasing rapidly in the time interval from $t = 0{\cdot}1$ to $t = 0{\cdot}2$. At $t = 0{\cdot}2$, the velocities are sufficiently small to be at the limit of permitted velocities for the current parameter régime. Comparison of the instantaneous streamlines at $t = 0{\cdot}1$ and $0{\cdot}2$ with and without solidification (as shown m Figure 5) clearly indicate the retarding of the flow by solidification. The loss of kinetic energy in the flow is due to the elevation of the effective zero in potential energy as the ice forms.

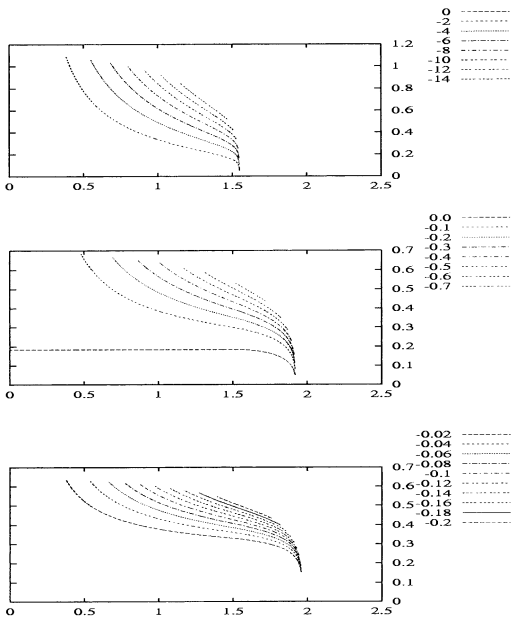

Figure 4. Instantaneous streamlines for the spreading and solidification of an axisymmetric drop of water with $B = 0$, $D \gg 1$ and $\lambda_f = O(D^{1/2})$ at times $t = 0$ (top), $t = 0{\cdot}1$ (middle) and $t = 0{\cdot}2$ (bottom). The solid/liquid interface corresponds to the zero isoline of the stream function. The streamlines are calculated using the leading-order balance in (36–37).

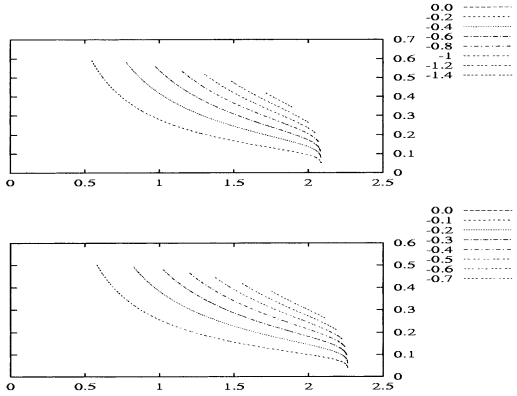

Figure 5. Instantaneous streamlines for the spreading of an axisymmetric drop of water without solidification at times $t = 0{\cdot}1$ (top) and $t = 0{\cdot}2$ (bottom). The solid/liquid interface ($z = 0$) corresponds to the zero isoline of the stream function. The streamlines are calculated using the leading-order balance in (36–37).

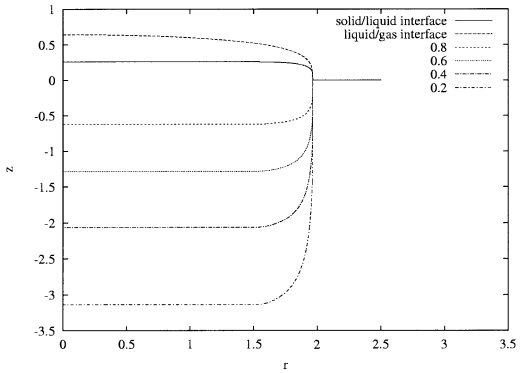

Figure 6. Propagation and solidification of an axisymmentric drop of water with $B = 0, D \gg 1$ and $\lambda_f = O(D^{1/2})$ at time $t = 0{\cdot}2$. Dimensionless temperature contours (using (50)) are shown alongside the solid/liquid and liquid/gas interfaces.

We do not specify the initial temperature distribution in the liquid. The rapid thermal conduction decreases the temperature in the liquid to the melting point on a short time-scale (see the inner expansion in Subsection 4.2). The temperature in the solid adopts an error function profile on this short time-scale. This temperature distribution matches into another slowly varying error function distribution on the long thermal time-scale (see the outer expansion in Subsection 4.2). Therefore, the heat flux into the substrate is significantly decreased on this long time-scale. The temperature contours at $t = 0{\cdot}2$ are shown in Figure 6. The thermal boundary layer is very thin near the front and grows as radius decreases. We note that the heat flux varies as a function of radius and time, taking its maximum value in the neighbourhood of the front. The use of a heat-transfer coefficient to model this flux would clearly be incorrect.

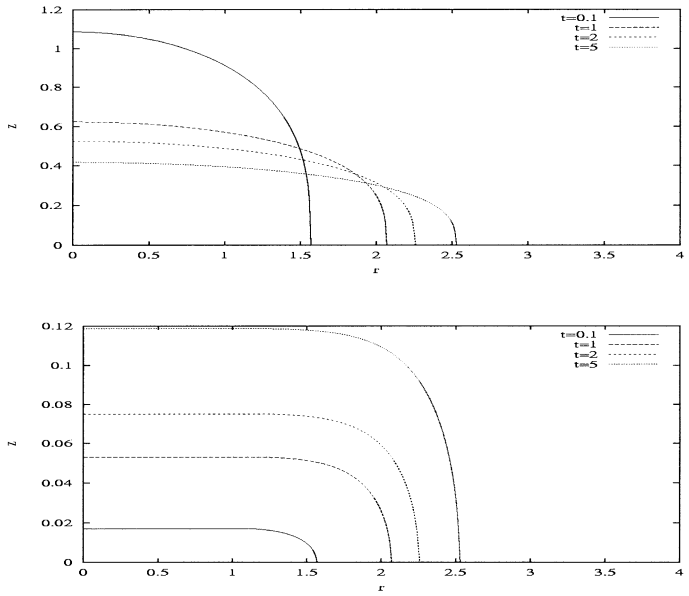

Figure 7. Basal solidification of an axisymmetric glycerol drop for the $V(t) = \bar{V}$ and $D \ll 1$ problem. The liquid/gas interface (top) corresponds to the solid/liquid interface (bottom). The interfaces are computed from (53–54) with $\hat{t} = 3(r/\hat{a})^8/(\Lambda \bar{V}^3)$ and (55).

5.2. SOLIDIFICATION OF GLYCEROL

Our next example concerns the initial stages of the solidification of a glycerol drop spreading over a horizontal plane of solid glycerol. If we take the physical properties of glycerol to be

$$\rho \sim 10^3 \text{ kgm}^{-3}, \quad c \sim 2 \times 10^3 \text{ Jkg}^{-1} \text{ K}^{-1}, \quad k \sim 0{\cdot}3 \text{ Js}^{-1} \text{ m}^1 \text{ K}^{-1},$$

$$\sigma \sim 6 \times 10^{-2} \text{ Nm}^{-1}, \quad \mu \sim 1 \text{ Nm}^{-2} \text{ s}, \quad L_f \sim 2 \times 10^5 \text{ Jkg}^{-1}, \quad T_m \sim 291 \text{ K},$$

(see, for example, [12, [13, pp. 15–16]) along with the scales of the initial conditions

$$a_0 \sim 10^{-1} \text{ m}, \quad U \sim 10^{-2} \text{ ms}^{-1}, \quad \delta \sim 10^{-1}, \quad T_m - T_a \sim 50 \text{ K},$$

then we obtain

$$\text{Re}\delta^2 \sim 10^{-2}, \quad C \sim 10^2, \quad G \sim 10^3, \quad \text{Pe} \sim 10^4, \quad D \sim 10^{-2}, \quad \lambda_f \sim 2.$$

These dimensionless constants fall into the parameter régime studied in Subsection 4.3.2. The basal solidification of an axisymmetric drop at different times is shown in Figure 7. The drop initially lies in the interval $0 \leq r \leq 1{\cdot}16$ and the solidification is independent of the radial coordinate r in this region. The coupling to the flow is through the location of the front which initiates the solidification at $r > 1{\cdot}16$ as it passes. Therefore, the front motion predicts the shape of the solid/liquid interface on this time-scale.

The rate of spreading is slowing significantly as time progresses in Figure 7. Our analysis predicts the final thickness of the solidified glycerol is of the order of $D^{1/6} \sim 10^{-1/3} \approx 0{\cdot}5$ spread over a region of the order of $D^{-1/12} \sim 10^{1/6} \approx 2$ on a long time-scale of the order of $D^{-2/3} \sim 10^{4/3} \approx 20$. This forecast compares reasonably with the initial stages of spreading in Figure 7.

6. Conclusions

New two-dimensional and axisymmetric continuum models have been derived to describe the effect of basal solidification on viscous gravity currents. Our first model incorporates a Stefan formulation for the basal solidification into the Navier-Stokes equations. After non-dimensionalisation, the Navier-Stokes equations are reduced in the lubrication and large-Bond-number limit. The coupling of gravity, viscosity and basal solidification is described by this second model. We note that both models contain two coupled moving boundaries.

In general, numerical methods are required to solve our system of equations. It is a non-trivial matter to obtain numerical solutions to coupled moving-boundary problems. However, analytical solutions may be obtained to the second model in three special cases:

(i) A similarity transformation may be obtained at zero Biot number in two cases. The two-dimensional problem when volume per unit length grows as time raised to the power 7/4 and the Julian number is large. The axisymmetric problem when volume grows as time raised to the power 3 and the dimensionless group $\nu g/Q$ is large. In both cases, the location of the front is proportional to time raised to the power 5/4, which is the same time dependence as without solidification. However, the constant of proportionality satisfies a modified system of equations; we anticipate that the front motion would be slower.

(ii) The parameter régime given by zero Biot number, large Stefan number and small modified Peclet number corresponds to leading-order coupling. Analytical progress is possible because the temperature of the fluid approaches the melting temperature over a short time-scale. The solid/liquid interface is then determined from the rate at which the latent heat is conducted into the solid over the long time-scale. Comparison of the spreading of a water drop with and without basal solidification indicates that the front is retarded by solidification. Indeed, the most dramatic result in this paper is that the front is arrested long before complete phase change has taken place (*cf.* [4] at small Bond number). The basal solidification is responsible for arresting the front motion, the solidification time-scale being shorter than the spreading time-scale in the neighbourhood of the front. The flow is also profoundly modified in magnitude and direction by the motion of the solid/liquid interface.

(iii) The parameter régime given by constant volume and large modified Peclet number corresponds to a weak coupling. The solidification depends on the fluid flow through the front position on the short time-scale, but the solidification does not modify the fluid motion at leading order. Over the long time-scale, the entire fluid volume solidifies. Although it is not possible to determine analytical solutions on this time-scale, scalings may be deduced. The final thickness of the solidified material is of the order of $a_o \mathrm{Pe}^{-1/7}\delta^{5/7}$ spread over a distance $a_0\mathrm{Pe}^{1/7}\delta^{2/7}$ for the two-dimensional problem and the final thickness of the order of $a_0\mathrm{Pe}^{-1/6}\delta^{2/3}$ spread over a radial distance $a_0\mathrm{Pe}^{1/12}\delta^{1/6}$ for the axisymmetric problem.

These solutions, in restrictive parameter régimes, provide valuable insight and may be used as a benchmark for future numerical studies.

We conclude by noting the importance of experiments to validate the models in this paper. The underlying assumption in the second model is that neglecting the boundary layer at the front and considering the outer expansion in the large-Bond-Number limit is a valid approximation. This assumption can only be verified by comparison with experiments. It would also be interesting to compare experimentally the constant of proportionality in the time dependence

of the front in solution (i) with and without solidification. Experiments are also necessary to examine the arresting of the fluid motion before complete phase change has taken place.

Acknowledgements

Financial support for the initial stage of this work was provided by the TMR contract entitled ‘Differential Equations in Industry and Commerce’.

References

1. H. E. Huppert, The propagation of two-dimensional and axisymmetric viscous gravity currents over a rigid horizontal surface. *J. Fluid Mech.* 121 (1982) 43–58.
2. L. M. Hocking, The spreading of a thin drop by gravity and capillarity. *Q. J. Mech. Appl. Math.* 36 1983) 55–69.
3. J. R. King, D. S. Riley and A. Sansom, Gravity currents with temperature-dependent viscosity. *Comp. Assist. Mech. Eng. Sci.* 7 (2000) 251–277.
4. S. Schiaffino and A. A. Sonin, Motion and arrest of a molten contact line on a cold surface: An experimental study. *Phys. Fluids* 9 (1997) 2217–2226.
5. M. Bunk, Spreading with basal solidification. Technical Report FZKA 6197, Forschungszentrum Karlsruhe (1999).
6. W. R. Smith, Models for solidification and splashing in laser percussion drilling. *SIAM J. Appl. Math.* 62 (2002) 1899–1923.
7. D. Snyder and S. Tait, A flow-front instability in viscous gravity currents. *J. Fluid Mech.* 369 (1998) 1–21.
8. B. Chalmers, *Principles of Solidification*. New York: John Wiley & Sons (1964) 319pp.
9. D. M. Anderson, M. G. Worster and S. H. Davis, The case for a dynamic contact angle in containerless solidification. *J. Crystal Growth* 163 (1996) 329–338.
10. G. K. Batchelor, *An Introduction to Fluid Mechanics*. Cambridge: Cambridge University Press (1967) 615pp.
11. P. Ehrhard and S. H. Davis, Non-isothermal spreading of liquid drops on horizontal plates. *J. Fluid Mech.* 229 (1991) 365–388.
12. G. W. C. Kaye and T. H. Laby, *Tables of Physical and Chemical Constants and Some Mathematical Functions*. London: Longman (1986) 477pp.
13. D. R. Lide, *CRC Handbook of Chemistry and Physics*. Boca Raton: CRC Press (2000)